An iterative technique for the reconstruction of residual stress fields in a butt-welded plate from experimental measurement, and comparison with welding process simulation

Chukkan, J. R., Wu, G., Fitzpatrick, M. E., Jones, S. & Kelleher, J.

Original citation & hyperlink:
Chukkan, JR, Wu, G, Fitzpatrick, ME, Jones, S & Kelleher, J 2019, 'An iterative technique for the reconstruction of residual stress fields in a butt-welded plate from experimental measurement, and comparison with welding process simulation' International Journal of Mechanical Sciences, vol. 160, pp. 421-428.
https://dx.doi.org/10.1016/j.ijmecsci.2019.07.001

DOI 10.1016/j.ijmecsci.2019.07.001
ISSN 0020-7403

Publisher: Elsevier

An iterative technique for the reconstruction of residual stress fields in a butt-welded plate from experimental measurement, and comparison with welding process simulation

Jazeel Rahman Chukkan , Guiyi Wu , Michael E. Fitzpatrick , Steve Jones , Joe Kelleher

PII: S0020-7403(19)31335-9
DOI: https://doi.org/10.1016/j.ijmecsci.2019.07.001
Reference: MS 5002

To appear in: *International Journal of Mechanical Sciences*

Received date: 17 April 2019
Revised date: 19 June 2019
Accepted date: 1 July 2019

Please cite this article as: Jazeel Rahman Chukkan , Guiyi Wu , Michael E. Fitzpatrick , Steve Jones , Joe Kelleher , An iterative technique for the reconstruction of residual stress fields in a butt-welded plate from experimental measurement, and comparison with welding process simulation, *International Journal of Mechanical Sciences* (2019), doi: https://doi.org/10.1016/j.ijmecsci.2019.07.001

Highlights

- Residual stress mapping provides an efficient alternative to welding process simulations.
- Upper bound distributions of experimental data secure conservatism in integrity assessments.
- Internal equilibrium in the FE model play important role in residual stress mapping.

An iterative technique for the reconstruction of residual stress fields in a butt-welded plate from experimental measurement, and comparison with welding process simulation

Jazeel Rahman Chukkan[a,b,1], Guiyi Wu[c], Michael E. Fitzpatrick[a], Steve Jones[a,2] , Joe Kelleher[d]

[a]Coventry University, Faculty of Engineering, Environment and Computing, Priory Street, Coventry, UK

[b]NSIRC, TWI Ltd, Granta Park, Great Abington, Cambridge, CB21 6AL, UK

[c]TWI Ltd, Granta Park, Great Abington, Cambridge, CB21 6AL, UK

[d]ISIS Pulsed Neutron & Muon Source, Harwell Campus, Didcot, Oxfordshire, United Kingdom

Abstract

Residual stress is a factor which potentially affects the integrity of welded components. We have developed a methodology of assessment to establish the state of residual stress in a butt-welded plate by using a limited set of experimental measurements obtained using neutron diffraction. The unique longitudinal and transverse residual stress components, as a result of the welding process, are measured across the weld in three depths through the thickness. The measured residual stresses are then used to estimate a stress distribution for each stress component. The estimated stress distribution is then mapped to a finite element model of the weld plate, before adopting an iterative solution to reconstruct the residual stress fields. In addition, a traditional welding simulation is performed using the same weld plate details to predict and compare the residual stress distributions. It is shown that accurate residual stress field reconstruction is possible in and around the area of measurement using the limited measurement data from the neutron diffraction technique. In the estimated stress profiles, an upper-bound distribution is implemented in the weld and Heat Affected Zone (HAZ). This increases the efficiency and reduces the complexity of modelling. In the meantime, conservatism in the estimated stress is secured.

KEYWORDS: Residual stress; Welding process modelling; Neutron diffraction; Residual stress mapping; Finite element method; Residual stress relaxation

[1] Corresponding author at: Faculty of Engineering, Environment and Computing, Coventry University, UK.
E-mail address: chukkanj@uni.coventry.ac.uk

[2] Present address: steve.jones@namrc.co.uk, Nuclear AMRC, University of Sheffield, Advanced Manufacturing Park, UK.

1. Introduction

Residual stresses are defined as the locked-in stresses in a solid body without any external loads present. Residual stresses are formed during welding due to nonhomogeneous plastic deformation during the process caused by high-temperature gradient and the difference in coefficient of expansion. Welding is one of the most common joining techniques used in engineering structures, some of which contain many miles of geometrically-constrained welding, resulting in complex residual stress distributions. Okawa et al. discussed the consequences of such stress distributions in ship structures (Okawa et al., 2006). Tensile residual stresses in welded components have a detrimental effect on the fatigue life. Modern structural integrity assessment procedures like BS 7910 ((BSI, 2015)), R6 ((R6 Revision 4, 2015)) and API 579 ((API 579-1, 2016)) require residual stress details in the structural integrity assessment: e.g., life assessment of a structure subjected to fatigue loading ((Withers et al., 2008)). It is difficult to quantify the residual stresses accurately in large and complex components without time-consuming and costly measurement programmes. Jun and Korsunsky pointed out that there are two main approaches to determine the full field of the unknown residual stresses in a component (Jun and Korsunsky, 2010). These are experimental measurement and deformation process modelling.

The experimental methods for the measurement of residual stresses are classified as either non-destructive or destructive. Complete experimental analysis of residual stresses, even in a simple geometric configuration like a butt joint, is prohibitively expensive and time-consuming as pointed out by Krawitz (Krawitz, 2011). Deformation process modelling or welding simulation, in this case, is one of the most common methods used for predicting and determining the residual stress distribution in a welded component. Weld modelling was initially developed based on analytical models of arc welding. Rosenthal initially proposed an analytical heat source model for welding, where he considered a point source moving on an infinite material (Rosenthal, 1946). However, the residual stress in the region where the point source is incident was inaccurate. Later Goldak et al. proposed a double-ellipsoidal model, which is a non-axisymmetric 3D heat source model suitable for simulating arc welds and welds produced by high-power-density processes (Goldak et al., 1984). Over the last few decades, with the advancement in computational capacity, there have been hundreds of papers on arc weld modelling, mainly to predict residual stresses and hence to optimise welding process parameters. Weld modelling essentially helps to replace, to an extent, the experimental work required in the development of new welding procedures. However, fracture and fatigue assessments, which require accurate weld residual stresses over a relatively small region of interest, often require welding process simulations, which can be complex and consume huge computational resource.

The residual stress mapping method proposed here is expected to fill this gap by reducing computation time whilst preserving the accuracy in determining the stress state in the region of interest.

On top of the experimental methods and deformation process modelling approach, another method for determining residual stress is to use a predictive method based on extracting a distribution of eigenstrain or inherent strains, as introduced by Mura (Mura, 1987), based on experimental measurements. The term eigenstrains as used by Mura (Mura, 1987) consists of all inelastic strains formed in a body due to various mechanisms such as phase transformation, purely-plastic flow and thermal expansion. Reißner was the first to use such inelastic strains to discuss misfit strains (Reißner, 1931). Recently, Lee et al. (Lee et al., 2018) used a simpler definition based on elastic energy, since residual stresses are formed due to the external and/or internal constraints in the eigenstrain region. One example of the application of the eigenstrain technique is the inverse eigenstrain method used by Jun and Korsunsky (Jun and Korsunsky, 2010) in which eigenstrains were estimated by analysing limited measurements. An eigenstrain distribution can be determined from an incomplete residual stress distribution in such a way that it is represented by a set of basic functions, which is called the inverse problem. Korsunsky (Korsunsky, 2009) performed finite element (FE) analysis in conjunction with minimisation of error with respect to experimental values and determined the complete eigenstrain distribution. A similar technique derives stress profiles that are analytically determined using both Airy's stress functions and experimental measurements. Farrahi et al. used this method to reconstruct residual stresses in an axisymmetric cylinder (Farrahi et al., 2009). Later, Farrahi et al. (Farrahi et al., 2010) extended this study to reconstruct residual stresses in a welded plate and Faghidian et al. (Faghidian et al., 2012) reconstructed residual stresses introduced in a steel beam by elastic-plastic bending.

Residual stresses can be predicted by virtual process modelling in a finite element (FE) model. Some finite element solvers like Abaqus and ANSYS have introduced this capability using user subroutines. Ficquet (Ficquet, 2007) introduced an iterative mapping procedure using predefined stress values in the FE analysis to estimate the complete residual stress field in a butt-welded plate with limited measurement values. Later, Do et al. (Do et al., 2013) mapped residual stresses on welded components where residual stresses were experimentally determined from deep-hole drilling measurements. This technique was also used by Coules et al. (Coules et al., 2014) for a geometry in which the incompatibility is confined in a small portion. Coules et al. (Coules et al., 2014) noted that the stress function method and inverse problems are most helpful if the residual stress or eigenstrain distributions can be parametrised accurately. However, the stress values mapped in these studies can lead to non-unique solutions in an FE solver due to the imbalance introduced with the stresses on a

small area. One of the inherent properties of residual stresses is that they should be self-balanced in the absence of any external loads. In almost every residual stress measurement experiment, an area with high residual stress is prioritised more than the areas with low residual stress. Therefore, the measurement data are usually incomplete. This leads to an unbalanced stress field if the data from the measurement are input into an FE model. The effect of incomplete residual stress measurements on the evaluation of stress intensity factor has been studied by Bao et al. (Bao et al., 2010).

In this work, an iterative technique is used to map residual stress values based on a self-equilibrating stress profile for a geometry with a large area of incompatibility. Even though the technique is suitable for a geometry with a small area of incompatibility, by using a self-equilibrating stress profile it was possible to achieve adequate accuracy in the residual stress distributions on and around the area of interest in a 3D finite-element model of a butt-welded plate. A numerical simulation is presented here in which the longitudinal and transverse residual stresses in a butt-welded specimen are mapped. Longitudinal residual stresses are the stress components along the weld, and transverse residual stress components are across the weld. The residual stress outputs from the mapping technique were compared with those obtained from welding process simulation and with experimental results measured using neutron diffraction. A comparison of the residual stress relaxation in the mapped model and weld model following one tensile load cycle with BS 7910 global relief is presented.

2 Methodology

2.1 Welding process and residual stress measurements

A multi-pass butt-welded plate of 400 × 140 × 12.7 mm^3 (length × width × thickness) was manufactured using the Gas-Metal Arc Welding process (ISO 4063-135) adopting a filler wire of diameter 1.2mm – classification EN ISO 14341-A (G 3Si1). The process used an argon-20% CO_2 gas mixture designated ISO 14175-M21 – ArC-20, which when combined with the current and wire-feed rate range used in this project was designed to achieve a minimum weld metal yield strength of 420MPa and a UTS range between 500 and 640MPa. No pre-heating of the DH36 steel substrate was necessary for this joint configuration due to the substrate thickness, carbon equivalent and arc energy used to meet the input guidance of BS EN 1011-2 (BS EN 1011-2:2001, 2004) for welding this steel grade.

A filler wire of 1.2 mm diameter, producing weld material with a yield strength of 450MPa, was used. The welding procedure specification is qualified in accordance with Lloyd's Register classification. The welding process set-up is shown in Figure 1a. Thermocouples of type-K and type-B, along with high-

temperature strain gauges, were used to monitor transient heat and strain variations. A special clamping arrangement, shown in Figure 1a, was manufactured to introduce maximum restraint while doing welding without introducing any unwanted movements on the thermocouples and the wires associated with them. The maximum restraint was imposed to represent the welding conditions encountered in fabricated ship structures. The welded plates were unclamped after welding. Electrical discharge machining (EDM) was employed to cut the butt-welded plates to prepare the specimen for study as shown in Figure 1b.

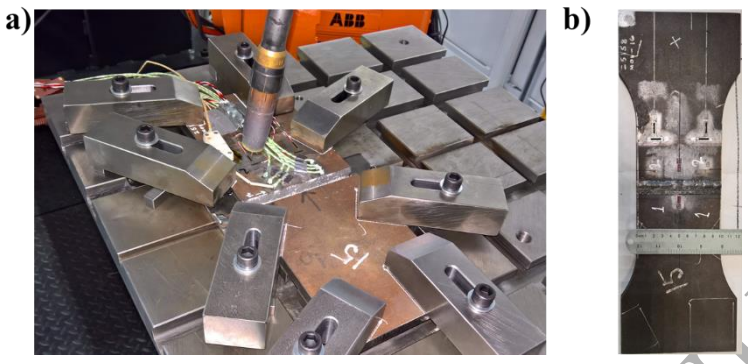

Figure 1: Specimen manufacturing a) Welding set-up with thermocouples and strain gauges b) Final specimen after EDM cut.

Residual stresses within the plate following welding and specimen preparation (EDM cut) were measured using neutron diffraction. Neutron diffraction is a non-destructive technique which can determine strains within the component. Neutron beams are highly penetrating and hence are capable of measuring strains through the thickness. The neutron diffraction peaks are used with Bragg's law (Bragg, 1929) to determine inter-planar lattice spacing. The lattice parameter of the stressed material is compared with a stress-free lattice parameter to determine internal strains within the material, as explained by Lodini (Lodini, 2003).

The time-of-flight neutron diffraction instrument ENGIN-X, at the UK's ISIS pulsed neutron source, was used to measure the lattice spacing (Santisteban et al., 2006). The primary flight path of the neutron beam in this instrument is 50m. The beam travels through a curved super mirrorguide to minimise the loss of neutrons in the travelled path. The ENGIN-X instrument has two detectors fixed at 90° angles to the incident beam, to provide two strain measurement directions along the scattering vectors Q_1 and Q_2 as shown in *Figure 2*. In *Figure 2* Q_1 corresponds to the strain parallel to the longer side received at the first detector bank, and Q_2 corresponds to the strain perpendicular to the longer side received at the second detector bank. In ENGIN-X, slits are motorised to enable control over the beam size in the vertical axis using a computer. Similarly, the secondary beam size is

defined based on the selected collimator. There are multiple collimators to define the secondary beam size having a fixed width (full width at half maximum) of 0.5, 1, 2, 3 and 4mm. In this work, all measurements were obtained using 3mm collimators.

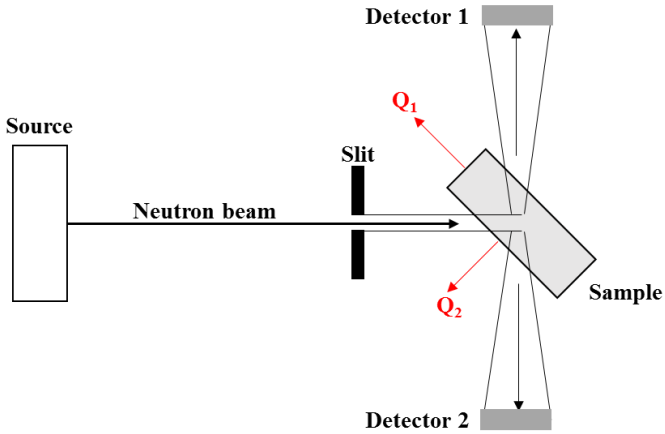

Figure 2: Schematic of time-of-flight neutron strain scanner ENGIN-X.

The measurement was obtained from a plane at the mid-thickness across the weld as shown in *Figure 3*. A gauge volume of $3 \times 3 \times 3$ mm^3 was used to obtain measurements from 30 points, illustrated in Figure *3*, from the measurement plane.

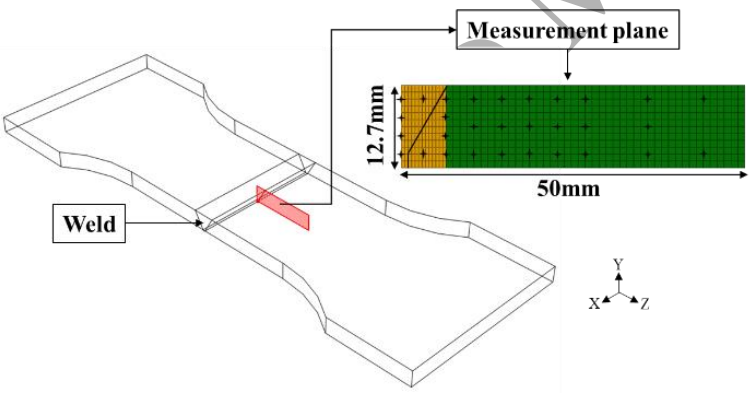

Figure 3: Neutron diffraction measurement locations on the mid-thickness of the specimen.

Three line-scans across the weld were performed at the mid-thickness plane of the specimen. The line scan locations were 2.5 mm below the top surface, at the mid-thickness, and 2.5mm above the bottom surface. Additionally, through-thickness measurements were performed at the weld centre and weld toe. A comb-like sample with a $4 \times 4 \times 10$ mm^3 (width × depth × height) was used as a stress-free sample as shown in Figure *4*. The comb-like sample was extracted from the same weld plate to help compare the measured lattice parameter

with the corresponding area in the stress-free sample. Eight measurement points were taken from the comb sample.

Figure 4: Comb-like reference sample used to determine stress-free lattice spacing and the neutron diffraction measurement locations on the reference sample.

The lattice parameters in three orthogonal directions at selected locations were measured using neutron diffraction. The lattice parameter in the butt-welded plate, d and the corresponding lattice parameter in the stress-free sample, d_0 is used to determine the residual strain at each location. The residual strain, ε and the error, $\Delta\varepsilon$ is determined using:

$$\varepsilon = \frac{d}{d_0} - 1 \tag{1}$$

$$\Delta\varepsilon = \left[\left(\frac{\Delta d}{d_0}\right)^2 + \left(\frac{d * \Delta d_0}{d_0^2}\right)^2\right]^{1/2} \tag{2}$$

where Δd and Δd_0 are the measurement errors in lattice parameter of the specimen and stress-free sample respectively. Further, the stress components were calculated using Hooke's law in its generalised expression:

$$\sigma_{xx} = 2\mu\varepsilon_{xx} + \phi\Delta$$
$$\sigma_{yy} = 2\mu\varepsilon_{yy} + \phi\Delta \tag{3}$$
$$\sigma_{zz} = 2\mu\varepsilon_{zz} + \phi\Delta$$

where $\mu = \frac{E}{2(1+\nu)}$, $\phi = \frac{\nu E}{(1+\nu)(1-2\nu)}$, $\Delta = (\varepsilon_{xx} + \varepsilon_{yy} + \varepsilon_{zz})$, E is the elastic modulus (210 GPa), v is the Poisson's ratio for steel (0.3) and x, y and z denotes any of the orthogonal directions relative to the plates reference shown in Figure *3*.

2.2 Welding process simulation

A sequentially coupled thermal/structural analysis is performed to simulate multi-pass Gas Metal Arc welding. Here heat transfer analysis results are predefined in a separate mechanical model to obtain stress results. The main steps involved in weld modelling are the introduction of arc-welding heat and the molten filler

metal into an FE model. An equivalent static heat source is used for arc-welding heat input. For filler metal deposition an element activation/deactivation technique is used where each weld pass is divided into small chunks. The detailed description of welding process modelling is explained as the 'Chunking' method in section III.15.4.5.3 of (R6 Revision 4, 2015). It is often simple to define a volumetric heat flux in multi-pass welding in comparison to a particular heat source model. It can be applied by simply dividing a weld pass into smaller weld blocks called 'weld chunks' and consider sequentially heating of each block in the weld material with a constant heat input. For example, on a welding process with two passes, each pass can be divided into N number of chunks introducing 2N number of chunks altogether. The heat flux, h (W/m^3), applied to a weld chunk can be defined as:

$$h = \frac{Q}{V_{wc}} \tag{4}$$

where V_{wc} is the volume of the weld chunks corresponding to a heating time Δt defined as:

$$\Delta t = \frac{L_{wc}}{\mathrm{v}} \tag{5}$$

where L_{wc} is the length of the weld chunks along the weld travel direction and v is the welding torch travel speed in m/s.

A Finite Element model of a rectangular weld plate of dimension 140 × 400 × 12.7 mm^3 was designed for the welding process simulations. The numerical simulation mesh details for both thermal and mechanical analyses were identical, and the model consisted of 654755 elements. 8-node linear heat-transfer brick elements and 8-node linear 3D stress elements were used for thermal and mechanical simulations respectively. Elements at the fusion zone (FZ) and heat-affected zone (HAZ) were very small to accommodate the high-temperature gradient and non-uniform thermal strain occurring. The thermophysical properties of the material were taken as temperature-dependent. The required material properties of DH36 were obtained from (Fu et al., 2014). In the mechanical analysis, a thermo-elasto-plastic material model with Von-Mises yield criterion associated to an isotropic hardening rule is used. Following unclamping after welding, EDM cutting of the plates was implemented in the weld FE model using element deactivation. The finite element solver used for all numerical computations is Abaqus Standard 6.14.

2.3 Residual stress prediction

2.3.1 Governing equations

In contrast to most earlier studies, this paper estimates a distribution by fitting experimental measurements of residual stresses for butt joints based on a profile introduced by (Masubuchi and Martin, 1966) which is given below.

$$\sigma_{res} = \sigma_m[1 - (\frac{z}{f_1})^2][e^{-0.5\,(\frac{z}{f_2})^2}] \quad (6)$$

where σ_{res} is the residual stress component, σ_m is the maximum residual stress (as high as the yield strength of the weld material in some cases). The parameters f_1 and f_2 define the width of the tension zone and compression zone of the residual stress component. Equ. 6 in its original form as introduced by (Masubuchi and Martin, 1966) has $f_1 = f_2 = f$. The co-ordinate z is defined as the distance across the weld as shown in Figure 5a. A residual stress profile was estimated based on experimentally measured residual stress values across the weld by solving f_1 and f_2 such that the estimated profile represents the measured values. Here it is assumed that the transverse and longitudinal components of residual stress are independent of the through-thickness axis of the plate.

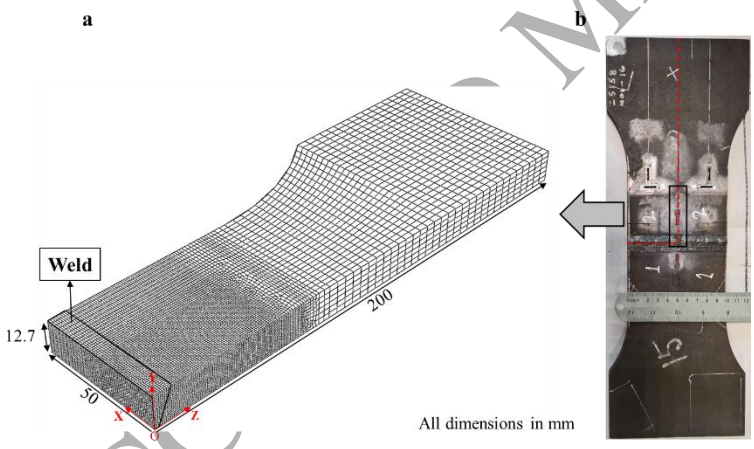

Figure 5: The butt-welded specimen design: (a) A quarter Finite Element (FE) model showing the dimension and meshing used for all iterations (b) A photograph of the butt-welded plate.

For a body containing residual stresses to be in equilibrium, based on small deformation theory, the body must satisfy the small-strain incompatibility condition. In the small deformation approximation, the total strain can be represented as the sum of elastic strain (***e***) and eigenstrain (ε^*) as given below:

$$\varepsilon = e + \varepsilon^* \quad (7)$$

Hence, in a linearly elastic material, the incompatibility introduced by eigenstrains can be defined as (Korsunsky, 2009):

$$\frac{\partial^2 e_{xx}}{\partial y^2}+\frac{\partial^2 e_{yy}}{\partial x^2}-2\frac{\partial^2 e_{xy}}{\partial x\partial y}=\Xi_1=-\frac{\partial^2 \varepsilon^*{}_{xx}}{\partial y^2}-\frac{\partial^2 \varepsilon^*{}_{yy}}{\partial x^2}+2\frac{\partial^2 \varepsilon^*{}_{xy}}{\partial x\partial y}$$

$$\frac{\partial^2 e_{yy}}{\partial z^2}+\frac{\partial^2 e_{zz}}{\partial y^2}-2\frac{\partial^2 e_{yz}}{\partial z\partial y}=\Xi_2=-\frac{\partial^2 \varepsilon^*{}_{yy}}{\partial z^2}-\frac{\partial^2 \varepsilon^*{}_{zz}}{\partial y^2}+2\frac{\partial^2 \varepsilon^*{}_{yz}}{\partial z\partial y}$$

$$\frac{\partial^2 e_{zz}}{\partial x^2}+\frac{\partial^2 e_{xx}}{\partial z^2}-2\frac{\partial^2 e_{xz}}{\partial x\partial z}=\Xi_3=-\frac{\partial^2 \varepsilon^*{}_{zz}}{\partial x^2}-\frac{\partial^2 \varepsilon^*{}_{xx}}{\partial z^2}+2\frac{\partial^2 \varepsilon^*{}_{xz}}{\partial x\partial z} \quad (8)$$

$$\frac{\partial^2 e_{xx}}{\partial y\partial z}+\frac{\partial}{\partial x}\left(-\frac{\partial e_{yz}}{\partial x}+\frac{\partial e_{zx}}{\partial y}+\frac{\partial e_{xy}}{\partial z}\right)=\Xi_4=-\frac{\partial^2 \varepsilon^*{}_{xx}}{\partial y\partial z}-\frac{\partial}{\partial x}\left(-\frac{\partial \varepsilon^*{}_{yz}}{\partial x}+\frac{\partial \varepsilon^*{}_{zx}}{\partial y}+\frac{\partial \varepsilon^*{}_{xy}}{\partial z}\right)$$

$$\frac{\partial^2 e_{yy}}{\partial x\partial z}+\frac{\partial}{\partial y}\left(\frac{\partial e_{yz}}{\partial x}-\frac{\partial e_{zx}}{\partial y}+\frac{\partial e_{xy}}{\partial z}\right)=\Xi_5=-\frac{\partial^2 \varepsilon^*{}_{yy}}{\partial y\partial z}-\frac{\partial}{\partial y}\left(\frac{\partial \varepsilon^*{}_{yz}}{\partial x}-\frac{\partial \varepsilon^*{}_{zx}}{\partial y}+\frac{\partial \varepsilon^*{}_{xy}}{\partial z}\right)$$

$$\frac{\partial^2 e_{zz}}{\partial x\partial y}+\frac{\partial}{\partial z}\left(\frac{\partial e_{yz}}{\partial x}+\frac{\partial e_{zx}}{\partial y}-\frac{\partial e_{xy}}{\partial z}\right)=\Xi_6=-\frac{\partial^2 \varepsilon^*{}_{zz}}{\partial x\partial y}-\frac{\partial}{\partial z}\left(\frac{\partial \varepsilon^*{}_{yz}}{\partial x}+\frac{\partial \varepsilon^*{}_{zx}}{\partial y}+\frac{\partial \varepsilon^*{}_{xy}}{\partial z}\right)$$

where $\Xi = [\Xi_1, \Xi_2, \Xi_3, \Xi_4, \Xi_5, \Xi_6]^{\mathrm{T}}$ is the forcing term which represents the incompatibility or residual stress in the object. In a fully compatible body, the forcing term, Ξ, is equal to zero. For a residually stressed body, in the absence of external loading, equilibrium can be defined as:

$$div\,\boldsymbol{\sigma}=0 \quad (9)$$

where $\boldsymbol{\sigma}$ is the stress tensor. For a linear-elastic material of stiffness tensor C, stress tensor can be defined using Hooke's law:

$$\boldsymbol{\sigma}=C:e \quad (10)$$

Equ. 10 implies that the residual stress fields in a solid body can be determined using the eigenstrain distribution and the elastic properties. Combining Hooke's law and the compatibility equations in conjunction with the known stress field, the forcing term Ξ can be determined. Considering the first compatibility equation, for an isotropic and linearly elastic material, the forcing term can be defined as:

$$\Xi_1=\frac{1}{E}\left|\frac{\partial^2}{\partial y^2}\left(\sigma_{xx}-\nu(\sigma_{yy}+\sigma_{zz})\right)+\frac{\partial^2}{\partial x^2}\left(\sigma_{yy}-\nu(\sigma_{zz}+\sigma_{xx})\right)-2(1-\nu)\frac{\partial^2 \tau_{xy}}{\partial x\partial y}\right| \quad (11)$$

where E is Young's modulus of the material, and v is Poisson's ratio. From Equ. 11, it can be concluded that the stress distributions from the experiment can be used directly in the FE model instead of eigenstrain distribution to generate a complete stress field.

2.3.2 Target residual stress field from measurements

Measured residual stresses were used to estimate a stress distribution based on Equ. 6. These distributions were used for the stress field reconstruction on the quarter FE model of the specimen shown in Figure 5a. The residual stress distribution estimated for both longitudinal and transverse residual stress was determined by varying parameters in Equ. 6 and minimising error against the measured values. The stress distributions presented below are estimated as the profile of the measured longitudinal (σ_{LR}) and transverse (σ_{TR}) residual stresses, respectively.

$$\sigma_{LR} = 450\left[1-\left(\frac{z}{16}\right)^2\right]exp\left[-\frac{1}{2}\left(\frac{z}{15}\right)^2\right] \quad (12)$$

$$\sigma_{TR} = 230\left[1-\left(\frac{z}{22}\right)^2\right]exp\left[-\frac{1}{2}\left(\frac{z}{13}\right)^2\right] \quad (13)$$

where σ_{LR} and σ_{TR} are the estimated longitudinal and transverse residual stresses which are shown in Figure *7* and Figure *8* respectively.

2.3.3 Iterative technique implementation

The estimated stress profile was mapped from x=0 to 25mm, y=0 to 12.7mm and z=0 to 45mm. A very fine mesh was used in the area where stresses are mapped. The mesh consisted of 83976, 20-node quadratic brick, reduced-integration elements. Routine scripts in Python code were used to write an input file for the solver in each iteration. The same Python code is programmed to read and post-process the results from the previous iteration. The implementation of FE analysis with the help of Python subroutine is shown in the flow chart illustrated in Figure *6*.

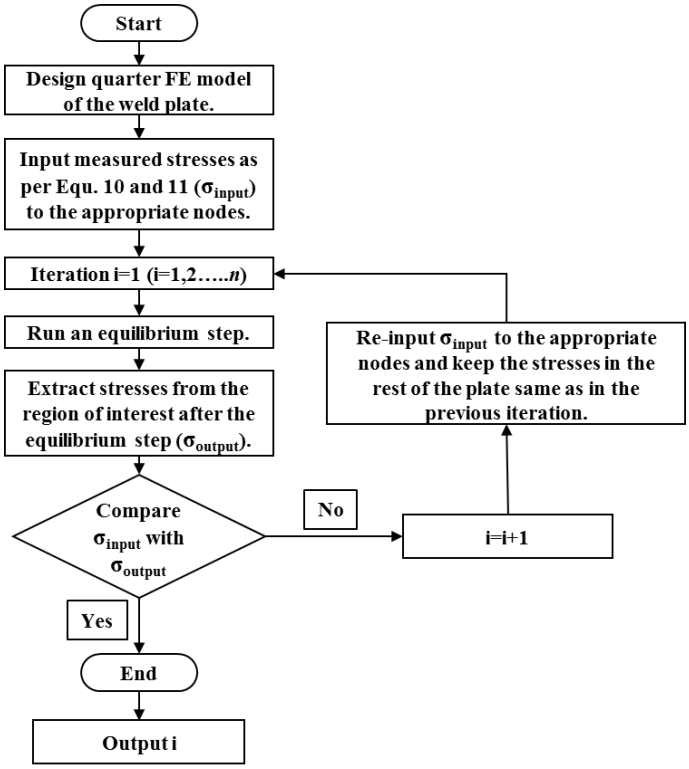

Figure 6: Flow chart illustrating the iterative finite element analysis.

For computational efficiency, a quarter FE model was implemented. In the first iteration, measured stresses were fitted based on Equ. 12 and 13 to obtain input, σ_{input}. The σ_{input} was pre-defined at the appropriate node locations (measured locations). An equilibrium step was run following initial stress pre-definition. In postprocessing, the stress distribution in the measured location, σ_{output} was extracted. The extracted output stresses were compared with the input stresses after each iteration. The initial few iterations were expected to redistribute the mapped stress to maintain equilibrium in the system because the mapping was only on a small region of the entire plate. In the first iteration, as a result of redistribution of stresses in the measurement locations following equilibrium step, residual stresses were generated on the area around the measurement location. If the input stresses, σ_{input} at the measurement location are seen redistributed, next iteration is run by re-inputting σ_{input} at the appropriate nodes while keeping the newly generated residual stress in the rest of plate as same as the last iteration. With each iteration, the deviation between input stress and output stress was decreasing. The analysis involved 75 iterations until the output stresses in the measurement locations were same as the input stresses.

Each iteration analysis consisted of two steps. In the initial step, all the measured stresses were predefined in the FE model. The second step was an equilibrium step in which the FE solver equilibrated the

stress throughout the specimen. For each iteration, the Python routine created a new solver file consisting of all the predefined stresses in the target zone and the stresses around the target area extracted from the previous iteration. The mesh throughout all iterations was not modified. In the case of all pre-definitions of the stress field, the averaged data were imposed element-wise at the integration points.

3 Results and discussion

3.3 Residual stresses from neutron diffraction

Longitudinal and transverse residual stress components were measured on the Y-Z plane in which line scans from z=0 to 42.5mm were performed at y=2.5 mm, y=6.35 mm and y=10.2 mm. The measured residual stress values at these locations in the plates are shown in Figure *7* and Figure *8*. The figures are plotted across the weld (in the Z direction in Figure *5*a) taken from: y=10.2mm, 2.5mm below the top surface; y= 6.35 mm, at the mid-thickness of the plate; and y=2.5 mm, 2.5mm above the bottom surface of the plate. Tensile residual stresses as high as the yield strength of the weld material and parent material are seen in the longitudinal component on and near the weld as shown in Figure *7*. Near the weld, the high tensile longitudinal residual stress is due to the balance between solidification of molten filler metal and shrinkage resistance of the base material. The high tensile stress then decreases to slightly compressive levels close to zero and finally becomes slightly tensile when going away from the weld centre. On the other hand, transverse residual stresses are lower than longitudinal residual stress but still significantly tensile in nature. Transverse residual stress in the line scan at y=2.5 mm have lower residual stresses of about 60MPa at the centre of the weld when compared to the measurements at y=6.35 and y= 10.2 mm as shown in Figure *8*. This can be due to the relatively small amount of filler metal deposition in the root pass and the low rate of cooling due to successive passes on top of it. This is true for the longitudinal stress components also; however, the heat transfer during welding is more across the weld than along the weld.

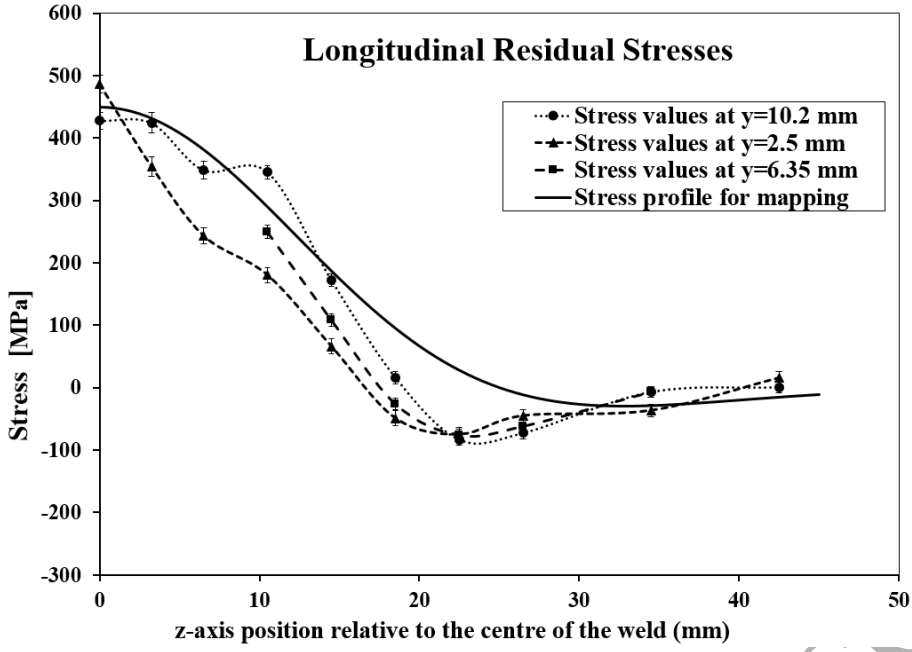

Figure 7: Longitudinal residual stress determined from neutron diffraction, and the stress profile used for mapping in the FE model determined using experimental data as per Equ. 12.

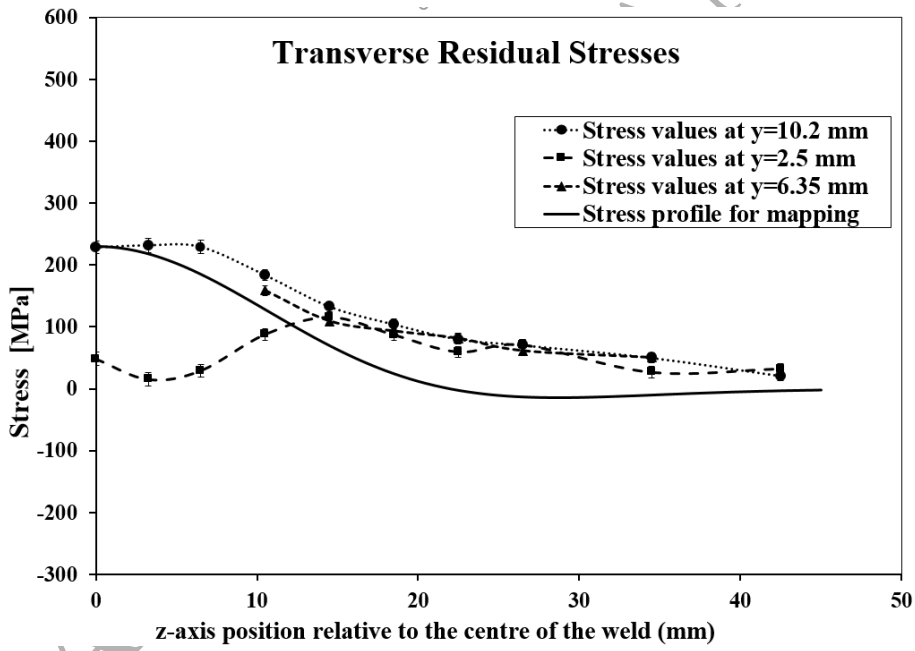

Figure 8: Transverse residual stress determined from neutron diffraction, and the stress profile used for mapping in the FE model determined using experimental data as per Equ. 13.

3.4 Numerical modelling results

3.4.1 Results of stress mapping

Stress mapping models were iterated 75 times until residual stress mapped were matching the estimated stress based on Equ. 12 and 13 and a stable residual stress profile was achieved overall. Figure 9 shows the longitudinal residual stress contour plot of the FE model after 75 iterations.

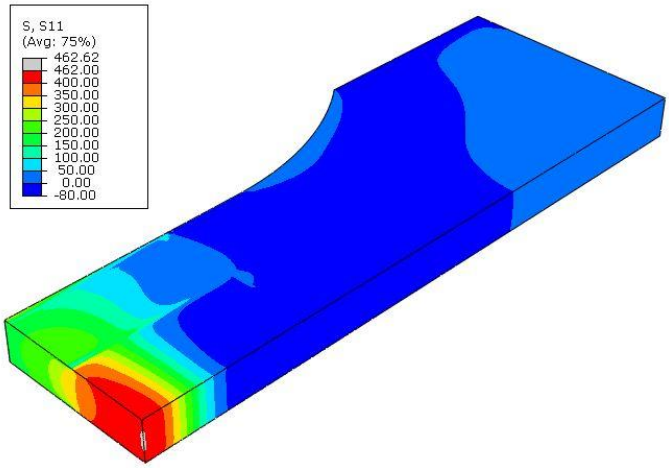

Figure 9: Reconstructed longitudinal residual stress contour obtained from stress mapping FE model after 75 iterations.

The stress field in the mapped area is completely reconstructed after the iterations, and Figure *10* and Figure *11* shows the comparison between longitudinal and transverse stress distribution in the measurement plane at y=6.35mm after the 1st and 75th iterations against the mapped stress profile. From the graphs, it can be noted that the stress mapping on the mapping plane matches with the required stress very well.

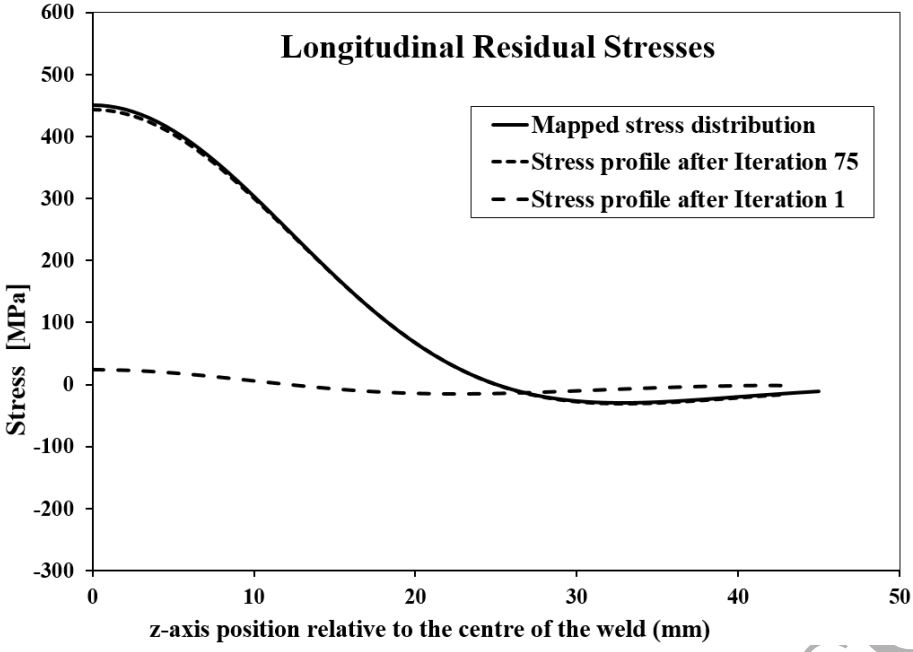

Figure 10: Comparison of input longitudinal residual stresses with stress mapping FE model output stresses after 1st and 75th iterations.

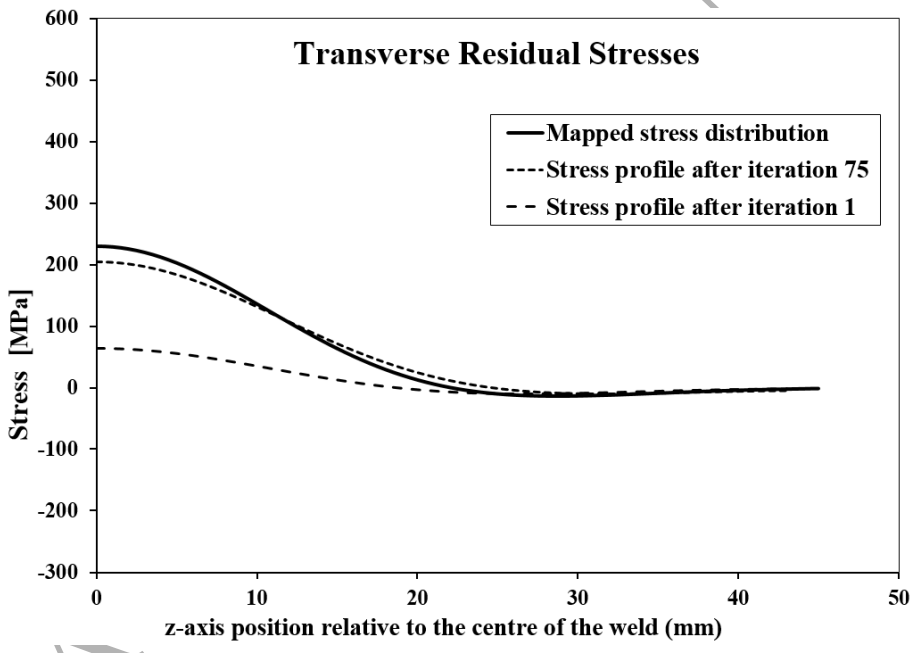

Figure 11: Comparison of input transverse residual stresses with stress mapping FE model output stresses after 1st and 75th iterations.

It is worth noting that this technique of residual stress field mapping is most accurate when the strain incompatibility is confined to a relatively small region such as a small weld. However, this method can be successfully employed in studies like engineering failure assessment in which accurate residual stress details are

required on a small region such as around a crack in a weld zone (fusion zone or heat affected zone). In cases where the focus is on the crack propagation, if the stress intensity factor due to residual stress can be determined correctly, the conservatism in the engineering critical assessment can be reduced.

3.4.2 Results of welding process simulation

A half of the welding FE model, following the element removal for the EDM cut, is shown in Figure *12* which shows a contour plot of longitudinal residual stress. Numerical predictions of the transverse and longitudinal residual stress profiles from the weld model at the same positions as the neutron diffraction measurements (y = 10.2 mm and y = 2.5 mm) were compared with the experimental data. Figure *13* and Figure *14* compare the measured stress values with the transverse and longitudinal stress components at the same locations from the weld model. The residual stress predicted in the weld model follows a similar trend to the experimental measurements. Except for the peak stress values away from the weld region, a good agreement is seen in the measured values and predicted stresses. The deviation in the values can be attributed to the EDM cutting before the measurements, restraints used in the experiments, and the material properties used in the FE model.

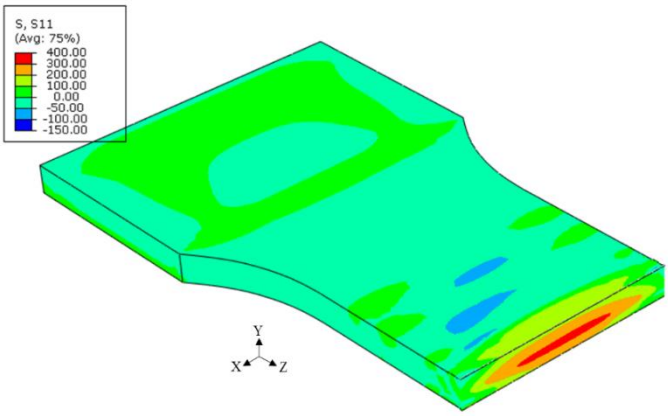

Figure 12: Longitudinal residual stress contour on half-model of the welding process simulation.

The welding process simulation in this work did not consider the influence of solid-state phase transformation that arises during heating and cooling in ferritic steels such as DH36 because the focus was on the analytical calculation of residual stress field based on the experimental measurement more than welding process simulation. However, it should be noted that in ferritic steels, if a significant amount of austenitic to ferritic phase transformation occurs before reaching room temperature, the ferrite phase will contract during cooling. At lower temperature, ferrite has higher yield strength than austenite, and hence, there will be less compensation of contraction strain by plastic relaxation (Bhadeshia, 2004, Rong et al., 2018). This phenomenon could give rise to

higher residual stresses after cooling. This could be a reason for the underprediction of the residual stresses on the weld and HAZ region.

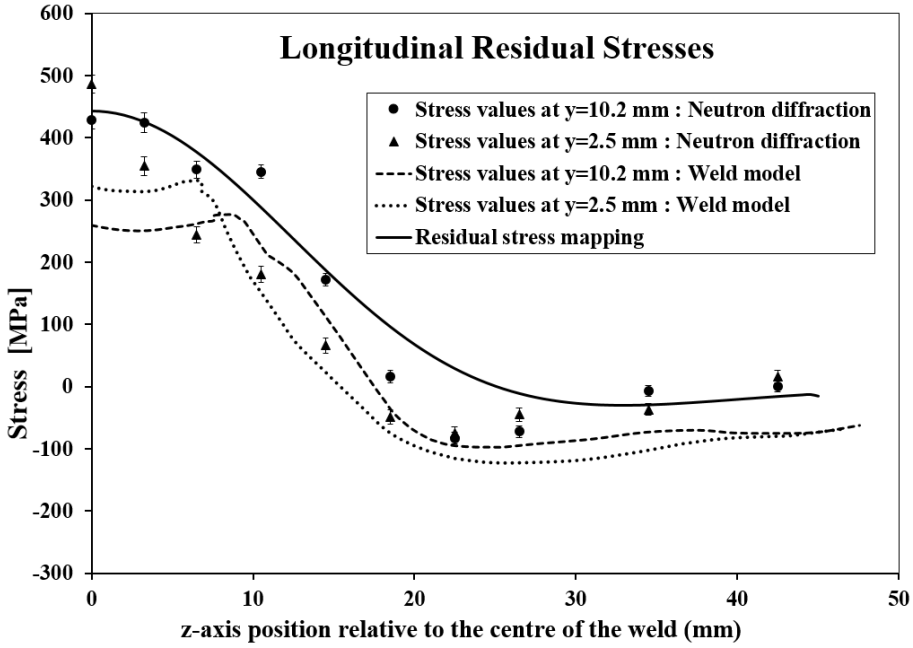

Figure 13: Comparison of longitudinal residual stress from experimental data, stress mapping FE model, and welding process simulation.

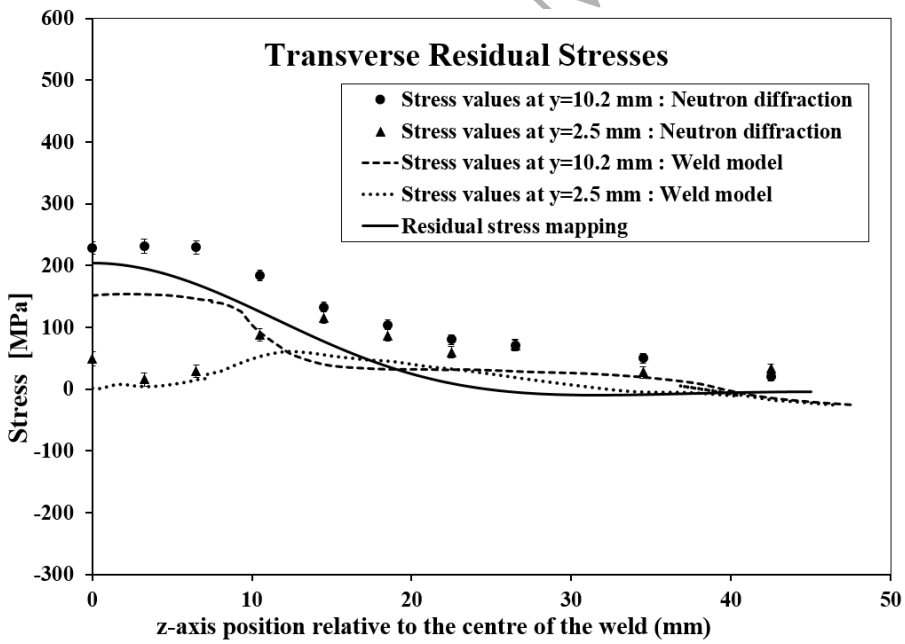

Figure 14: Comparison of transverse residual stress from experimental data, stress mapping FE model, and welding process simulation.

In the present study, longitudinal and transverse residual stresses are represented as a stress distribution function (Equ. 12 and Equ. 13 respectively) to determine stress values at locations between two measurement points so that unique values are mapped on to a set of elements in the FE model. Therefore, it is emphasised that the stress values measured need to be represented in a distribution function. Residual stress measurement of locations on a line scan with very small increments is often prohibitively expensive and time-consuming. This suggests that the residual stress measurement experiments can be planned in such a way that more of the measurement locations contain the inherent strains.

Again, this method is dependent on the number of stress components being mapped. In this paper, only two orthogonal stress components, longitudinal and transverse components, were used. The third orthogonal component in the through-thickness direction in a plate is usually fairly low. However, to increase the accuracy of mapping, alternative approaches currently being looked into including through-thickness components as well. For more complex geometries such as T-joints or a plate with multiple welds, more measurement data are required than the case of a simple butt joint.

3.5 Effect of loading on pre-existing residual stress field

A Finite-element model was implemented to apply a single load cycle on both the weld model and the mapped FE model, to compare the feasibility of using the mapped model data in post-analysis of relaxation of residual stress. Both models were subjected to a single tensile load cycle of 0 to 330 to 0 kN to introduce maximum stress of 260 MPa across the weld toe plane. The loading is applied across the weld, along the z-axis. The relaxation in the longitudinal and transverse residual stress distribution along the measurement plane is shown in Figure *15* and Figure *16* respectively.

BS 7910 assumes some global relief of residual stresses on welded structures when subjected to primary loading (BSI, 2015). The relaxation in the transverse residual stress in the weld model and the mapped model is compared with the BS 7910 global relief method in Figure *16*. Longitudinal and transverse residual stress distributions after a load cycle from both numerical models show good agreement. There are some deviations in the case of longitudinal components near the weld-to-base-plate interface. Figure *16* shows the as-welded stress distribution as recommended for a butt-welded plate, and the stress relaxation after global relief due to the applied load. The stress profile as recommended from BS 7910 is highly conservative when compared with the measured transverse residual stress. The weld and weld toe regions are critical in crack initiation, and in the case of the estimated stress profile, the conservatism is secure at the weld region and represents the actual scenario

better than BS 7910. After a cyclic load, the level of relaxation in the weld model and mapped model is about 56% and 70% respectively.

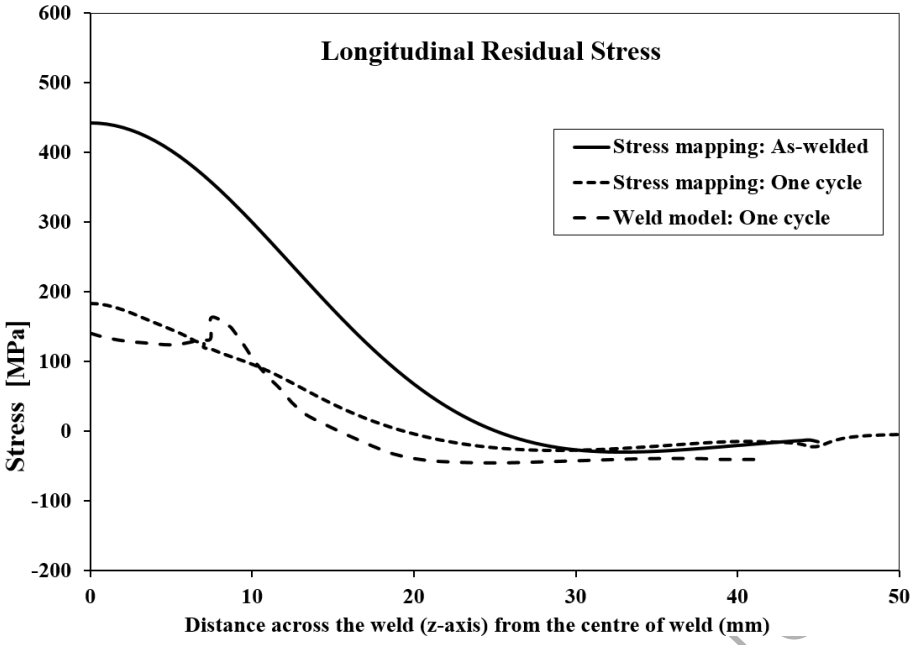

Figure 15: Longitudinal residual stress relaxation after a load cycle from FE model

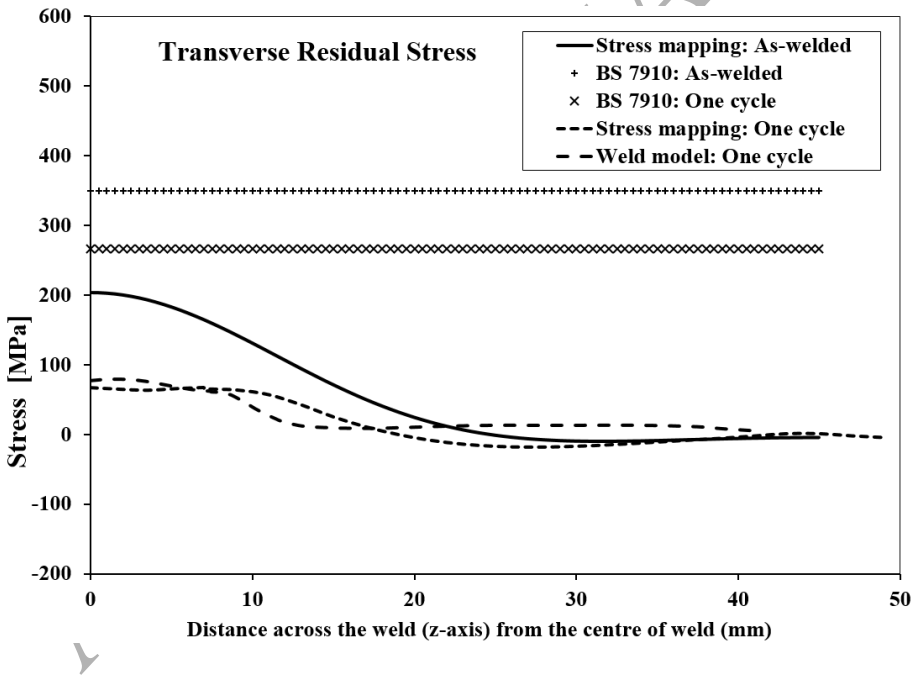

Figure 16: Comparison of transverse residual stress relaxation after a load cycle from the FE model and BS 7910 global relief rule.

Conclusions

Residual stress mapping in a butt-welded plate using a limited number of stress data measured using neutron diffraction was achieved using a self-balancing stress distribution in a finite element model. A weld process simulation was also implemented, and comparison is drawn between the predicted residual stresses from a full analytical weld FE model and the mapped stresses. A single load cycle was applied on both weld and mapped FE models and compared with the BS 7910 global relief rule. The conclusions drawn from this study are:

- Self-balancing stress equations can play an important role in supporting residual stress mapping techniques such as neutron diffraction, where data are typically obtained from a relatively small region of interest only.
- Analytical weld modelling is still one of the best methods to generate the complete stress field on a weld plate. However, the computational efficiency of the residual stress mapping technique was much better than full welding process modelling. For fracture or fatigue analysis of welded structures, in which the area of potential crack initiation is identified, the mapping technique can increase the computational efficiency considerably without losing accuracy.
- The as-welded residual stresses as recommended by BS 7910 are at the yield strength of the base plate. This is hence considered conservative. An upper-bound residual stress distribution can be estimated to implement in a finite element model using the residual stress mapping technique in this paper. This increases the efficiency and reduces the complexity of modelling. By using an upper bound distribution based on measured residual stresses, the conservatism in the stress will be secure.
- A good agreement is seen between the stress relaxation after one load cycle in the weld model and mapped model. A comparison of the relaxation of transverse residual stresses with BS 7910 global relief method shows that the standard method is overly conservative in the treatment of stress relaxation after loading.

In summary, the mapping method using a combination of limited experimental data and stress balance is a simple and computationally efficient method for the prediction of the global residual stress field for a relatively simple geometry. Further study is required to assess its applicability to more complex geometries with multiple weldments.

Acknowledgements

This publication was made possible by the sponsorship and support of Coventry University, and the Lloyd's Register Foundation, a charitable foundation helping protect life and property by supporting engineering-related education, public engagement, and the application of research. The work was enabled through, and undertaken at, the National Structural Integrity Research Centre (NSIRC), a postgraduate engineering facility for industry-led research into structural integrity established and managed by TWI Ltd through a network of both national and international Universities.

References

API 579-1. Fitness-For-Service. 3rd ed. : American Petroleum Institute; 2016.

Bao R, Zhang X, Yahaya NA. Evaluating stress intensity factors due to weld residual stresses by the weight function and finite element methods. Eng. Fract Mech 2010;77:2550-66.

Bhadeshia H. Developments in martensitic and bainitic steels: role of the shape deformation. Materials Science and Engineering: A 2004;378:34-9.

Bragg WL. The Diffraction of Short Electromagnetic Waves by a crystal. Proceedings of the Cambridge Philosophical Society 1929;23:153.

BS EN 1011-2:2001. Annex C. In: British Standards, editor. Welding- Recommendations for welding of metallic materials, Part 2: Arc Welding of ferritic steels. : British Standards Institute; 2004. p. 15.

BSI. 7910: Guide to methods for assessing the acceptability of flaws in metallic structures. British Standards Institute 2015.

Coules HE, Smith DJ, Abburi Venkata K, Truman CE. A method for reconstruction of residual stress fields from measurements made in an incompatible region. Int J Solids Structures 2014;51:1980-90.

Do S, Serasli K, Smith D. Combined measurement and finite element analysis to map residual stresses in welded components. ASME Pressure Vessels and Piping Conference 2013;V-6B:pp:V06BT06A065.

Faghidian SA, Goudar D, Farrahi GH, Smith DJ. Measurement, analysis and reconstruction of residual stresses. The Journal of Strain Analysis for Engineering Design 2012;47:254-64.

Farrahi G, Faghidian S, Smith D. An inverse method for reconstruction of the residual stress field in welded plates. Journal of Pressure Vessel Technology 2010;132:061205.

Farrahi GH, Faghidian SA, Smith DJ. Reconstruction of residual stresses in autofrettaged thick-walled tubes from limited measurements. International Journal of Pressure Vessels and Piping 2009;86:777-84.

Ficquet X. Development and application of the deep hole drilling method. University of Bristol 2007.

Fu G, Lourenco MI, Duan M, Estefen SF. Effect of boundary conditions on residual stress and distortion in T-joint welds. Journal of constructional steel research 2014;102:121-35.

Goldak J, Chakravarti A, Bibby M. A new finite element model for welding heat sources. Metallurgical and Materials Transactions B 1984;15:299-305.

Jun T, Korsunsky AM. Evaluation of residual stresses and strains using the Eigenstrain Reconstruction Method. International Journal of Solids and Structures 2010;47:1678-86.

Korsunsky AM. Eigenstrain analysis of residual strains and stresses. The Journal of Strain Analysis for Engineering Design 2009;44:29-43.

Krawitz AD. Neutron Strain measurement. Materials Science and Technology 2011;27:589-603.

Lee S, Coratella S, Brügger A, Clausen B, Brown D, Langer K, et al. Boundary Effects in the Eigenstrain Method. Exp Mech 2018;58:799-814.

Lodini A. Calculation of residual stress from measured strain. In: Fitzpatrick ME, Lodini A, editors. Analysis of residual stress by diffraction using neutron and synchrotron radiation. : Taylor and Francis; 2003. p. 47-59.

Masubuchi K, Martin DC. Investigation of Residual Stresses in Steel Weldments. Ship Structure Commitee 1966;SSC-174 Final Rpt.

Mura T. Micromechanics of defects in solids. 2nd ed. : Martinus Nijhoff Publishers, Dordrecht; 1987.

Okawa T, Sumi Y, Mohri M. Simulation-based fatigue crack management of ship structural details applied to longitudinal and transverse connections. Mar Struct 2006; 19:217-40.

R6 Revision 4. Assessment of the integrity of structures containing defects. United Kingdom: EDF Energy Nuclear Generation Ltd; 2015.

Reißner H. Eigenspannungen und Eigenspannungsquellen. Z angew Math Mech 1931; 11:1-8.

Rong Y, Lei T, Xu J, Huang Y, Wang C. Residual stress modelling in laser welding marine steel EH36 considering a thermodynamics-based solid phase transformation. International Journal of Mechanical Sciences 2018;146-147:180-90.

Rosenthal D. The Theory of Moving Sources of Heat and Its Applications to Metal Treatments. Transactions of the ASME 1946; 68:849-866.

Santisteban J, Daymond M, James J, Edwards L. ENGIN-X: a third-generation neutron strain scanner. Journal of Applied Crystallography 2006; 39:812-25.

Withers PJ, Turski M, Edwards L, Bouchard PJ, Buttle DJ. Recent advances in residual stress measurement. Int J Pressure Vessels Piping 2008; 85:118-27.

Figure captions

Figure:1- Specimen manufacturing a) Welding set-up with thermocouples and strain gauges b) Final specimen after EDM cut.

Figure:2- Schematic of time-of-flight neutron strain scanner ENGIN-X.

Figure:3- Neutron diffraction measurement locations on the mid-thickness of the specimen.

Figure:4- Comb-like reference sample used to determine stress-free lattice spacing and the neutron diffraction measurement locations on the reference sample.

Figure:5- The butt-welded specimen design: (a) A quarter Finite Element (FE) model showing the dimension and meshing used for all iterations (b) A photograph of the butt-welded plate.

Figure:6- Flow chart illustrating the iterative finite element analysis.

Figure:7- Longitudinal residual stress determined from neutron diffraction and the stress profile used for mapping in the FE model determined using experimental data as per Equ. 10.

Figure:8- Transverse residual stress determined from neutron diffraction, and the stress profile used for mapping in the FE model determined using experimental data as per Equ. 11.

Figure:9- Reconstructed longitudinal residual stress contour obtained from stress mapping FE model after 75 iterations.

Figure:10- Comparison of input longitudinal residual stresses with stress mapping FE model output stresses after 1st and 75th iterations.

Figure:11- Comparison of input transverse residual stresses with stress mapping FE model output stresses after 1st and 75th iterations.

Figure:12- Longitudinal residual stress contour on half-model of the welding process simulation.

Figure:13- Comparison of longitudinal residual stress from experimental data, stress mapping FE model, and welding process simulation.

Figure:14- Comparison of transverse residual stress from experimental data, stress mapping FE model, and welding process simulation.

Figure:15- Longitudinal residual stress relaxation after a load cycle from FE model.

Figure:16- Comparison of transverse residual stress relaxation after a load cycle from the FE model and BS 7910 global relief rule.